

## Article

# Comparison of Surface and Spectral Properties of Optical Sensor Layers Prepared by Spin/Spray Coating and Printing Techniques

Nena Dimitrušev<sup>1,2,3,\*</sup>, Polonca Nedeljko<sup>2</sup>, A. F. P. Allwin Mabes Raj<sup>2,4,5</sup> and Aleksandra Lobnik<sup>2,3</sup><sup>1</sup> Messer Slovenija, Jugova Ulica 20, 2342 Ruše, Slovenia<sup>2</sup> Institute for Environmental Protection and Sensors, Beloruska 7, 2000 Maribor, Slovenia<sup>3</sup> Faculty of Mechanical Engineering, Centre of Sensor Technology, University of Maribor, Smetanova 17, 2000 Maribor, Slovenia<sup>4</sup> Department of Environmental Science, Jožef Stefan Institute, Jamova 39, 1000 Ljubljana, Slovenia<sup>5</sup> Jožef Stefan International Postgraduate School, Jamova 39, 1000 Ljubljana, Slovenia

\* Correspondence: nena.dimitrusev@messergroup.com

**Abstract:** This study investigated the surface properties of optical sensor layers prepared using sol-gel technology and their response to dissolved NH<sub>3</sub>. A glass substrate was used to fabricate the optical sensor layers. The sol-gel solution was applied to the glass substrate using three different techniques: spin coating (SC), inkjet printing (IP), and spray coating (SP). In this work, we have attempted to investigate the effects of the different techniques for producing the sensor layers and to determine their response in the presence of ammonia. The surface properties (surface free energy—SFE and surface chemical composition—XPS) and spectral properties (response to ammonia and real-time response) of the prepared optical sensor layers were characterised. The results show that the sensor layers prepared by different techniques have similar SFE and XPS values, but different responses to dissolved NH<sub>3</sub> solution and different responses in real-time measurements (exposure to fresh fish). Sensor layers prepared with a spray coating (SP) are the most responsive, the most sensitive, and have a higher response over time and the biggest colour change compared to SC and IP sensor layers.

**Keywords:** optical sensor layers preparation; spin coating; spray coating; inkjet printing; SFE; XPS; NH<sub>3</sub> response; real-time response



**Citation:** Dimitrušev, N.; Nedeljko, P.; Mabes Raj, A.F.P.A.; Lobnik, A. Comparison of Surface and Spectral Properties of Optical Sensor Layers Prepared by Spin/Spray Coating and Printing Techniques. *Chemosensors* **2023**, *11*, 136. <https://doi.org/10.3390/chemosensors11020136>

Academic Editor: Ilaria Rea

Received: 3 November 2022

Revised: 31 January 2023

Accepted: 7 February 2023

Published: 13 February 2023



**Copyright:** © 2023 by the authors. Licensee MDPI, Basel, Switzerland. This article is an open access article distributed under the terms and conditions of the Creative Commons Attribution (CC BY) license (<https://creativecommons.org/licenses/by/4.0/>).

## 1. Introduction

Compared to conventional electrical sensors, the advantages of optical chemical sensors are insensitivity to electromagnetic interference, selectivity, and safety when working with flammable and explosive compounds. They are widely used because of their many capabilities, such as sensitivity, cost-effectiveness, and non-destructiveness. The sol-gel process offers a simple and easy way to obtain thin films with high purity, homogeneous composition, and good properties in just one step and at a low cost [1].

The basis to produce optical chemical sensors is usually an indicator dye, which is immobilized in the corresponding polymer base according to the chosen immobilization method. The properties of the sol-gel material and its final shape can be influenced by various process parameters. A major influence on the final properties of the optical sensor is the immobilization of the indicator in a suitable polymer carrier, which can be in the form of thin membranes—sensor layers, gels, optical fibers, parts, etc.-etc. Thin polymeric supports are most used to produce sensor layers. The sensing layers can be produced by various application techniques. However, the sensory properties of optical chemical sensors can also be altered by the technique of applying the sol-gel solution to a suitable substrate.

Optical chemical sensors can be found in various fields, such as medicine, biotechnology, personal protection, and the chemical industry. Recently also for medical applications

such as disease diagnosis from breath analysis [2]. Optical chemical sensors can be manufactured by various methods, but in recent years the sol-gel method is one of the most used techniques. The sol-gel method allows the fabrication of optical sensors and biosensor layers for the measurement of pH, gas vapours and ionic species, as described by Jeronimo et al. [3]. Other reports over 10 years (2005–2015) deal with sol-gel-based optical sensor layers (absorption and luminescence) for analytes such as oxygen, pH, ammonia, carbon dioxide and heavy metal ions [1,4]. Optical pH sensor based on sol-gel was also investigated by Zhang et al. [5]. Different sensors from different research groups were developed in the environmental field: Biring et al. [6] develop dual gas sensors for the simultaneous detection of oxygen and ammonia gases, and optical hydrogen sensors were developed by a group of Matsuura et al. [7]. For the detection of hydrogen peroxide was developed ratiometric fluorescence sensors based on CgSe/ZnS quantum dots by Doung et al. [8].

In environmental protection, monitoring environmental parameters is crucial to control or limit excess concentrations that can be lethal to living organisms. One of these parameters is ammonia gas (NH<sub>3</sub>), which occurs naturally in the atmosphere and is also widely used in various industrial and agricultural activities. In most cases, ammonia is used in the production of fertilizers and other chemical substances. Existing and standardized methods for determining the concentrations of various environmental parameters are time-consuming and require specialized sample preparation and highly skilled personnel. Therefore, there is a need to develop alternative methods for the determination of environmental parameters with analytical devices that are small and portable and allow the acquisition of analytical signals on-site, continuously (online), and at remote locations. Optical chemical sensors are one such alternative.

The most used techniques for the preparation of sensors are spin coating, dip coating, inkjet printing, and, in recent years, most commonly, spray coating. **Spin coating** is currently the laboratory standard for the rapid development of small-area films from solution [9] and has been used to produce uniform coatings of desired thickness [10]. However, the spin-coating technique has a lot of disadvantages, such as large amounts of waste [9,10] and incompatibility with reel-to-reel or large-area processing [9,11,12]. It is not readily scalable [9]. The spin coating technique is also more sensitive to variations in precursor compositions, resulting in sharper changes in the size of surface features [13]. The biggest problem of the spin coating technique is problematic manufacture in a large area, while inkjet printing and spray coating are techniques that can fulfil all requirements for large-scale production [14].

**Inkjet printing** is an important tool in industrial mass fabrication and one of the most versatile methods available for prototyping [15]. It is used in research laboratories for the fabrication of (bio)chemical sensing devices or single functional elements of such devices [16]. With inkjet printing, electronic data can be transferred to paper or overhead transparencies. It is one of the key technologies in the field of defined polymer deposition [17]. More recently, inkjet technology used in the fields of electronics and mechanics has been adopted for the deposition of biological reagents onto surfaces. This kind of printing involves the digitally controlled ejection of drops of fluid from a print head onto a substrate [18]. The inkjet printing system is simple, rapid [15,19,20], low cost, high resolution, flexible, and non-contact, and generates a low amount of waste [15,16,20,21]. It also allows room temperature deposition, applies to large areas and flexible substrates [20], and all the controlled deposition of small droplets of liquids (ink) onto a substrate [16,21]. The system is compatible with paper substrates and amenable to pattern formation [19]. The disadvantages of this system are that the short gelation time of silica sols can cause gelation and clogging of the inkjet nozzles [19], cavitation bubbles, undesired satellite drops, nozzle clogging, droplets instabilities, agglomeration, precipitation, or deposition of solutes [21]. Printability problems may occur when the particle size becomes of the order of 1 µm [17]. Rheological properties, such as viscosity and surface tension, are the most critical part of the formulation of the bio-ink [18,19]. A low ink viscosity can cause uneven jetting, but if

the ink is too viscous, jetting will not occur [18]. The surface tension is responsible for the spheroidal shape of the liquid drop emerging from the nozzle [17,18].

Because of the disadvantages of these two techniques, the use of **Spray coating** for large-scale production of materials with different coatings is increased. Spray coating has many advantages compared with other techniques, namely: the ability to coat complex geometries at an industrial scale [1,22] and the ability to coat large surfaces with different morphologies and roughness [1]. During the deposition of the material, the amount discarded is minimized [11], and that's what makes these techniques promising to substitute the spin coating technique [10]. With the spray coating technique, we can generate very thin layers on different substrates, which is promising for the industrial application of organic-inorganic thin films [22]. It is also very promising for large-area deposition with controlled thickness [9–11]. Thicknesses ranging from 250 to 450 nm can be produced with a single-pass spray process [11] and it is not directly proportional to the number of layers but to the deposited mass [23]. Using spray coating, different thicknesses can be achieved by changing different parameters, but the most important are pressure [1,22] and the distance between the extreme of the gun and the target [1,10,22]. How deposition occurs depends also on the speed of the gun in the lateral movement ( $x$ -axis), the distance between depositions in the  $y$ -axis [22], the fluid viscosity, and the shape and size of the nozzle (size is usually fixed by the spray gun) [1]. The amount that can be applied to the surface depends on the nozzle speed ( $s$ ), flow rate (FR) (i.e., rate of liquid ejection from the spray nozzle), and nozzle height ( $h$ ) (distance from the substrate) [24]. The latter (distance from the substrate) has a great impact on the morphology of the deposited layer [10]. By changing parameters such as distance and speed of depositions, roughness can be changed. At larger distances and higher speeds, the surface roughness decreases [1].

In Table 1, we list the sensors for  $\text{NH}_3$  (gas or aqueous) prepared with different coating techniques (spin coating, spray coating etc.).

**Table 1.** Comparison of sensing characteristics of various sensors for  $\text{NH}_3$  detection in different media, prepared with coating techniques.

Material	Method	Media	LOD (ppm)	Response Time (s)	Recovery Time (s)	Ref.
3% Er-doped ZnO	Nebulizer spray	gas	125	120	10	[25]
CA matrix	Spin coating	gas	/	1320	3600	[6]
Sol-gel	coating	aqueous	0.2	300	/	[26]
WO <sub>3</sub> /Si; WO <sub>3</sub> /PS	spin coating	gas	/	16.1; 14.1	19.7; 19.2	[27]
1D supramolecular nanofibres	drop-casting	humidity	<1 ppb	2.05	2.25	[28]
Pani-SnO <sub>2</sub> Nanocomposite	Spin coating	gas	/	12–15	80	[29]
Sol-gel	Spin coating	gas	34	<600	480	[30]
$\alpha$ -Fe O <sub>2</sub> 3-ZnOsol-gel	Spin coating	gas	/	20	20	[31]
ZnO	Spray pyrolysis	gas	/	20	25	[32]
Sol-gel	Spray coating	aqueous	0.1	5	1500	Present work

Polyaniline-based ammonia gas sensors were investigated [14]. The authors prepared ammonia gas sensors with spray coating and inkjet printing and concluded that the different roughness of the layers made with inkjet printing did not contribute to a change in sensor performance.

Although measuring the contact angle and hydrophilicity/hydrophobicity of sol-gel films is critical for many sensing applications [4], there is very little, almost no, research on how surface properties affect the responsiveness of optical sensing layers and how different sensor fabrication techniques affect responsiveness.

The novelty of this study is the comparison of the surface properties of sensor layers prepared by three different deposition techniques: spin coating (SC), inkjet printing (IP) and spray coating (SP) and the simultaneous monitoring of the effects of different deposition techniques on the response of the sensor in the presence of dissolved ammonia (NH<sub>3</sub>). This work may be useful for a deeper understanding of the fact that different preparation techniques of sensor layers have different effects on their response in the presence of the analyte.

## 2. Materials and Methods

### 2.1. Preparation of Optical Sensor Layers

In this study, a glass substrate ( $d = 20.0$  mm, thickness = 1.6 mm) was used as a solid support onto which the sol-gel solution was applied. The glass substrate was activated by treatment with concentrated nitric acid (65%; HNO<sub>3</sub>) for 24 h, then washed with distilled water and ethanol and dried at 70 °C for 24 h. Afterwards, the glass substrate was prepared for sol-gel application using various techniques. The sensor solutions were prepared by combinations of hydrophilic and hydrophobic sol-gel precursors and absorption indicator dyes. The sol-gel process was carried out using an acid-catalysed method. Detailed information on the composition of the sol-gel solutions is confidential.

Sensor layers were prepared with three different techniques: spin coating, inkjet printing and spray coating.

#### 2.1.1. Spin Coating

Sensor thin layers were prepared using a WS-650MZ-23NPP/LITE spin coater from Laurell Technologies Co. (Lansdale, PA, USA). A 100 µL aliquot of the solution was spread on a glass substrate and spin-coated at a maximum of 1500 rpm for 30 s. The prepared optical sensor layers were marked as Sensor\_SC.

#### 2.1.2. Inkjet Printing

Inkjet printing was carried out using a Dimatix inkjet printer (DMP-2831) with DMP-2800 series software (Fujifilm Dimatix Inc., Santa Clara, CA, USA). For printing, a 10 pL cartridge was used and optical sensor layers were printed using 50 µm of Drop spacing. The prepared optical sensor layers were marked as Sensor\_IP.

#### 2.1.3. Inkjet Printing

For spray coating was used an automatic self-made system equipped with an Airbrush spray gun and Inkscape vector graphics software. Optical sensor layers were prepared with one sprayed layer and 1 bar of pressure with a 10 cm distance between the gun and glass substrate. The prepared optical sensor layers were marked as Sensor\_SP.

### 2.2. Characterization of Optical Sensors

In this study, the surface properties of the prepared optical sensor layers with different techniques were studied. The spectral properties were also studied through the determination of the responsiveness of the optical sensors in an aqueous medium, and the real-time response with the determination of the colour of tested optical sensors on the responsiveness to fresh fish.

A schematic representation of the response of the optical sensors to NH<sub>3</sub> is presented in Figure 1.

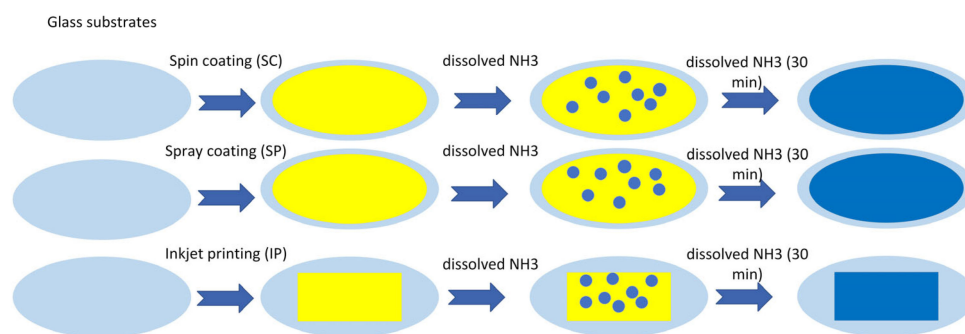


**Figure 1.** Schematic representation of the response of the optical sensors to  $\text{NH}_3$ .

### 2.2.1. ATR-FTIR Spectroscopy

ATR-FTIR were recorded on a Perkin Elmer spectrometer. The absorbance measurements were carried out within the range of  $450\text{--}4000\text{ cm}^{-1}$  with 16 scans and a resolution of  $4\text{ cm}^{-1}$ .

### 2.2.2. Surface Free Energy (SFE)

The surface free energy was calculated with contact angle (CA) measurements and surface-free energy (SFE) calculations. For the CA measurements, an OCA5 contact-angle measurement system from Dataphysics (Filderstadt, Germany) was used. CA was determined from the tangent of the sessile drop profile at the three-phase contact point drawn onto the photoprint. This method was used for the surface free energy calculation, using three different liquids: Milli-Q water, diiodomethane, and formamide. The total SFE ( $\gamma_{\text{TOT}}$ ) was calculated according to [33] and the SFE components were then calculated according to [34]. Total surface free energy is divided into Lifshitz–van der Waals interactions ( $\gamma_{\text{LW}}$ ) and acid-based interactions ( $\gamma_{\text{AB}}$ ). Lifshitz–van der Waals interactions comprise dispersion, dipolar, and induction interactions, while acid-based interactions comprise all the electron donor–acceptor interactions, like hydrogen bonding. The acid–base interactions are also subdivided into electron donor  $\gamma_{\text{S}}^-$  (Lewis base) and electron acceptor  $\gamma_{\text{S}}^+$  (Lewis acid) parts [34].

### 2.2.3. Surface Chemical Composition (XPS)

Surface chemical composition with determining amounts of differently bound carbons was investigated with X-ray photoelectron spectroscopy (XPS) using a PHI-TFA XPS spectrometer produced by Physical Electronics Inc. (Chanhassen, MN, USA). For the analysis, a sensor area of 0.4 mm in diameter was used. A pass energy of 29 eV (using an energy analyzer operating at a resolution of 0.6 eV) was used to acquire the high-energy resolution spectra, with an accuracy of the binding energy of about 0.3 eV. Surface composition was quantified from XPS peak intensities considering relative sensitivity factors provided by the instrument manufacturer [35].

### 2.2.4. Avantes AvaSpec Spectrophotometer

The spectral properties (absorbance measurements) of the optical sensor layers in the presence of ammonia were performed with an Avantes AvaSpec spectrophotometer. The spectrophotometer was connected to a flow cell that has been custom designed. An optical chemical sensor was placed in the flow cell and the sample solution was let into the cell. Using a peristaltic pump (Heidolph Pumpdrive 5001) the flow rate of the sample solution was kept constant and was  $7.5\text{ mL/min}$ . The spectrophotometer used an AvaLight DHC-light source. The detector was set to 10 ms integration time with 40 cycles and the number of points for smoothing the spectral data was set to 5. For generating the analytical signal Avasoft 7.6 software was used.

With the system, the Avantes AvaSpec spectrometer also determined the response time (Time drive) of prepared sensor layers in buffer pH7 and a certain concentration of

ammonia ( $5 \times 10^{-3}$  M  $\text{NH}_4\text{Cl}$ ). To this end,  $5 \times 10^{-3}$  M  $\text{NH}_4\text{Cl}$  was dissolved in pH7 buffer from a stock 0.1 M solution of ammonium chloride in pH7 buffer. We started with the introduction of the pH buffer and after 10 min, the signal was stable. Then, we alternately added  $5 \times 10^{-3}$  M  $\text{NH}_4\text{Cl}$  and buffer pH7 for 30 min each, two times.

### 2.2.5. Real-Time Response of Optical Sensors

The real-time response of the prepared optical sensor layers was determined using EOPTIS CLM19x colourimeter analysis. Optical sensor layers were exposed to fresh fish (from the market) in a closed container under real conditions in the refrigerator. The colour change of the sensor layers in the container in the presence of fish was measured daily.

## 3. Results

### 3.1. Preparation of Optical Sensor Layers with Different Techniques

In this article, we present three different techniques to produce optical sensor layers: spin coating, inkjet printing, and spray coating. All techniques are suitable to produce optical sensor layers. The optical sensor layers produced using the three different techniques are shown in Figure 2.

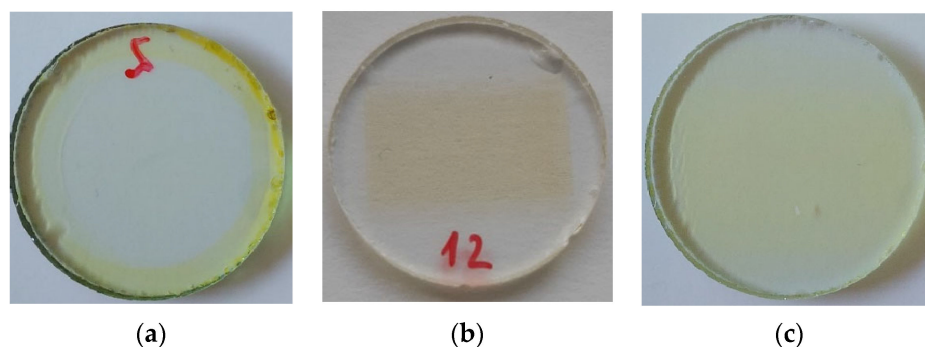


**Figure 2.** Optical sensor layers produced on glass substrates using three different techniques: (a) spin coating (SC), (b) inkjet printing (IC), and (c) spray coating (SP).

It can be seen from Figure 2 that all sensor layers have a light-yellow colour and a thin layer. In the case of the optical sensor layers produced by coating (spin coating and spray coating), the entire glass surface is covered with the solution, while in the case of the optical sensors produced with the inkjet printing process, only the centre is covered in the form of a rectangle that was used for printing. The sensor layers produced with the spin coating (Figure 2a) are slightly yellow in the middle and more intensely yellow at the edges. The coating also has a very flat surface. The sensor layer produced with inkjet printing (Figure 2b) has a rectangle shape and the entire rectangle is covered with solution. These optical sensor layers are thicker and rougher and have a distinct roughness. The sensor layer produced with spray coating (Figure 2c) has a flat surface that is completely covered with the solution.

### 3.2. Characterization of Optical Sensor Layers

#### 3.2.1. ATR-FTIR Spectroscopy

ATR-FTIR spectroscopy was used to confirm the efficiency of the preparation of optical sensor layers on glass carriers. The results are represented in Figure 3. Only the region from  $2000 \text{ cm}^{-1}$  to  $500 \text{ cm}^{-1}$  is shown.

Figure 3 shows the FTIR spectra of optical sensor layers prepared on a glass substrate using the three different techniques. The spectra of the differently prepared sensor layers are represented by different coloured lines: without application of sol-gel solution (pure glass—black line), spin coating (SC—red line), inkjet printing (IP—blue line), and spray coating (SP—green line).

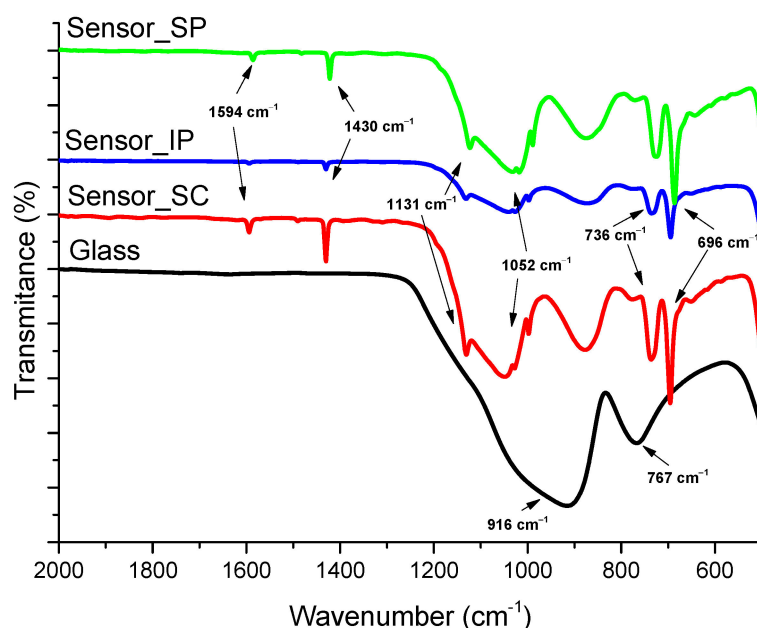


**Figure 3.** FTIR spectra of pure glass substrates without application of the sol-gel solution (pure glass—black line) and sol-gel coated glass substrates: spin coating (SC—red line), inkjet printing (IP—blue line), and spray coating (SP—green line).

Two peaks are visible on the spectrum of the pure glass substrate (black line). The first peak is at  $916\text{ cm}^{-1}$ , characteristic of Si-O-Si (oxygen-silicon bond) and the second peak is at  $767\text{ cm}^{-1}$ , characteristic of Si-O vibrations [36]. In the other three cases, where the sensor layers were prepared using different application techniques, identical peaks were present. The only difference is in the intensity of the peaks, which is the least intense in the case of the sensor coating produced with the inkjet printing technique (blue line). In all four spectra, the same peaks are seen in the range from  $1250\text{ cm}^{-1}$  to  $700\text{ cm}^{-1}$  characteristic of silica [37], while the range around  $1430\text{ cm}^{-1}$  to  $1625\text{ cm}^{-1}$  is characteristic of C-C stretches in the region [38]. The peak at around  $1600\text{ cm}^{-1}$  is characteristic of C-C in the ring [39]. The peak at around  $1430\text{ cm}^{-1}$  is characteristic of the stretching of silicon attached to the ring (Si-C<sub>6</sub>H<sub>5</sub>) [39,40]; the peak at  $1130\text{ cm}^{-1}$  is characteristic of Si-O-Si asymmetric stretching [40] or Si-O-CH<sub>3</sub> [39] and the peak at around  $1050\text{ cm}^{-1}$  is characteristic of Si-O-C stretching [40]. The peaks at  $736\text{ cm}^{-1}$  and  $696\text{ cm}^{-1}$  are characteristic of ring breathing [37], which is presented in ormosil and used for preparing optical sensor layers.

ATR-FTIR spectroscopy confirmed that the glass substrate was successfully covered with solution (for preparation of optical sensor layers) with the presentation of the same functional groups on all optical sensor layers.

### 3.2.2. Water Contact Angle and Surface Free Energy

#### Hydrophilic/Hydrophobic Character of Glass and Optical Sensor Layers Prepared with Different Techniques

The hydrophilic/hydrophobic character is calculated by the water contact angles (WCA) measurements. The results for the uncoated glass and glass substrates with optical sensor layers prepared by the three different techniques are shown in Table 2 and are the average of at least five measurements.

From Table 2, it can be seen that the uncoated glass substrate has a very small water contact angle of  $21.19 \pm 0.63^\circ$ . This indicates a hydrophilic character of the optical sensor layers, because of the presence of silanol groups (Si-O-H) on the surface of glass [41], also proved by FTIR analysis (Figure 3).

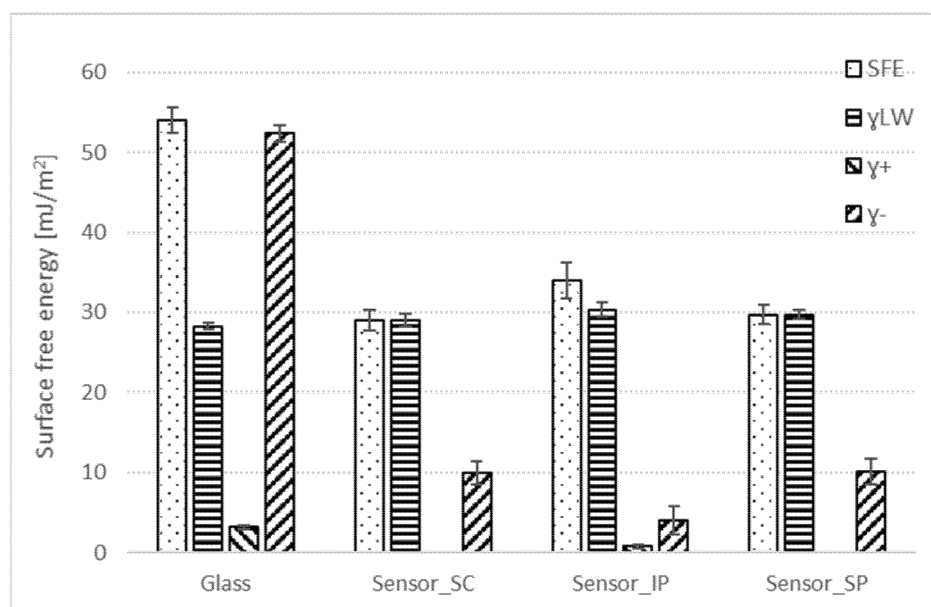
**Table 2.** Water contact angles (WCA) of substrates and optical sensor layers prepared with different techniques: spin coating (Sensor\_SC), inkjet printing (Sensor\_IP), and spray coating (Sensor\_SP).

Samples	Water Contact Angles (°)
Glass	21.19 ± 0.63
Sensor_SC	79.84 ± 1.41
Sensor_IP	83.69 ± 2.46
Sensor_SP	80.06 ± 1.36

The optical sensor layers made with spin coating and spray coating have almost the same hydrophilic/hydrophobic character, with a contact angle of 80°, while the optical sensor layers made with inkjet printing have a higher contact angle of around 84°. This is probably due to the higher roughness of the surfaces of the optical sensor layers made by inkjet printing. Films made by Inkjet printing have high visible roughness. The roughness was so large it was impossible to measure with the AFM technique. Kangur et al., reported that high contact angle and high surface roughness are more or less correlated [42]. The reason for the higher contact angle with water in the case of the optical sensor layers is also a result of nonpolar groups presented in the ormosils used for making sensors (Figure 3).

#### Surface Free Energy of Glass and Optical Sensor Layers Prepared with Different Techniques

The results of surface free energy (SFE) calculations of the substrate and optical sensor layers prepared with different techniques are represented in Figure 4. There are represented total surface free energy ( $\gamma_{\text{TOT}}$ ) and Lifshitz–van der Waals contributions ( $\gamma_{\text{LW}}$ ), which represent the nonpolar part and the polar part, which is divided into the electron-donor contribution ( $\gamma^-$ ) and the electron-acceptor contribution ( $\gamma^+$ ).

**Figure 4.** Surface free energy of glass and optical sensor layers prepared with different techniques: spin coating (Sensor\_SC), inkjet printing (Sensor\_IP), and spray coating (Sensor\_SP).

All these parameters are calculated from contact angle measurements with three test liquids performed using goniometry. These liquids are water, formamide, and diiodomethane.

The SFE ( $\gamma_{\text{TOT}}$ ) of the glass substrate is the highest at  $53.99 \pm 1.63 \text{ mJ/m}^2$ , with the highest electron donor ( $\gamma^-$ ) component ( $52.36 \pm 1.02 \text{ mJ/m}^2$ ). This is considered a high-energy surface.

The surface free energies of the optical sensor layers prepared with spin coating and spray coating are the same, with an SFE ( $\gamma_{\text{STOT}}$ ) of around  $29 \text{ mJ/m}^2$ , which is smaller by around 45% in comparison with the glass substrate. The electron donor component ( $\gamma^-$ ) is around  $10 \text{ mJ/m}^2$  and is smaller by around 80% in comparison with the glass substrate. Lifshitz–van der Waals contributions ( $\gamma_{\text{LW}}$ ) are around  $30 \text{ mJ/m}^2$  and are increased by around 2.6% for optical sensor layers made by spin coating and 5.2% for optical sensor layers made by spray coating.

From all SFE results, optical sensor layers made with inkjet printing have the highest SFE ( $\gamma_{\text{STOT}}$ ), at around  $34 \text{ mJ/m}^2$ , and the lowest electron donor component, around  $4 \text{ mJ/m}^2$ . The total SFE ( $\gamma_{\text{STOT}}$ ) is smaller by around 37% and the electron donor component is smaller by around 92% in comparison with the glass substrate.

### 3.2.3. X-ray Photoelectron Spectroscopy (XPS)

X-ray photoelectron spectroscopy was used to determine the surface elemental composition and relative amounts of differently bound carbons in the glass and optical sensor layers prepared with different techniques: spin coating, inkjet printing, and spray coating. The results are represented in Tables 3 and 4.

**Table 3.** Surface elemental composition of the substrate (glass) and optical sensor layers prepared with different techniques: spin coating (Sensor\_SC), inkjet printing (Sensor\_IP), and spray coating (Sensor\_SP).

Samples	Atomic Proportion (at. %) of Surface Composition			
	C	O	Si	O/C
Glass	47.4	34.8	15.2	0.73
Sensor_SC	63.5	22.4	14.1	0.35
Sensor_IP	61.6	24.1	14.2	0.39
Sensor_SP	64.6	22.5	12.8	0.35

**Table 4.** Relative amounts of differently bound carbons obtained from the XPS survey spectra for the glass and optical sensor layers prepared with different techniques: spin coating (Sensor\_SC), inkjet printing (Sensor\_IP), and spray coating (Sensor\_SP).

Samples	C1 (%)	C2 (%)	C4 (%)
	C-C; C-H	C-O; C-OH; C-Si	O-C=O
Glass	88.5	6.9	4.6
Sensor_SC	91.0	9.0	0
Sensor_IP	93.2	6.8	0
Sensor_SP	91.2	8.8	0

Different elements presented on the surface of the glass are characteristic of the substrate material. The O/C ratio of glass is 0.73, which means that glass is hydrophilic, which is proved by the measurements of the hydrophilic/hydrophobic character and the polar component of the surface free energy (Table 2 and Figure 4).

Optical sensor layers made with spin coating and spray coating have almost identical surface elemental composition, while optical sensor layers made by inkjet printing are a little different but still broadly the same. All optical sensor layers contain about 62–64 at. % of C, 22–24 at. % of O and 12–14 at. % of Si. The O/C ratio is also the same. In all cases, the amount of C is increased by more than 30% and the content of O decreased for almost the same amount. The Si content also decreased by around 7% in the case of spin coating and inkjet printing and by around 16% in the case of spray coating. The O/C ratio also decreased to around 47% in the case of optical sensor layers prepared with inkjet printing

and to around 52% in the case of optical sensor layers prepared with coating techniques. The O/C ratio indicates that the surfaces of all optical sensor layers are more hydrophobic, which is proved by the determination of SFE (Figure 4).

From Table 4 we can see that relative surface carbon amounts involved in the C-C bonds in the case of optical sensor layers are higher compared to the glass substrate, and the C-O, C-OH, and C-Si carbon fractions also increased. The glass substrate contains carboxylic O=C=O groups. The presence of carboxylic groups is responsible for the hydrophilic character of the glass substrate (Table 2) and the highest O/C ratio (Table 3).

From these results, we can also see that using different techniques for preparing optical sensor layers did not affect the differently bonded carbon atoms. All optical sensor layers have similar surface chemical characteristics. In all cases, C atoms are bonded similarly: C-C and C-H bonds represent around 90% of C-atoms and 6–10% are bonded in C-O/C-OH/C-Si bonds.

Optical sensor layers prepared with coating techniques (spin and spray) have higher carbon amounts involved in the C-C bond by around 3%, meanwhile optical sensor layers prepared with inkjet printing the figure is 5%. Carbon fractions of C-O, C-OH, and C-Si are for optical sensor layers prepared with coating techniques higher by around 30% and for optical sensor layers prepared with inkjet printing smaller by around 1%.

These results are in good correlation with the SFE results (Figure 4). The portions of carbon involved within the C-C bonds on the surface of the glass substrate is 88.5% and on the surface of optical sensor layers prepared with different techniques is more than 91%. This means that optical sensor layers have a bigger amount of C-C bonds compared to a glass substrate by 2.8% and 3% in the case of optical sensor layers prepared with spin coating and spray coating respectively and by around 5% in the case of optical sensor layers prepared with inkjet printing. At the same time, the Lifchitz–van der Waals contribution ( $\gamma_{sLW}$ ) of the surface free energy is bigger by 2.6% in the case of optical sensor layers prepared with spin coating, 5.2% in the case of optical sensor layers prepared with spray coating and 7.4% in the case of optical sensor layers prepared with inkjet printing. The glass substrate has carbon fractions involved within the C-OH and O=C-O bonds of about 6.9 and 4.6%, respectively. The content of these polar groups proves that the glass substrate has a hydrophilic character. This is also proved by the O/C ratio, which is 0.73. Optical sensor layers prepared with different techniques had no O=C-O groups, but optical sensor layers prepared with coating techniques have a bigger amount of C-OH and C-Si groups by around 30%. Optical sensor layers prepared with inkjet printing have almost the same amount of C-OH and C-Si groups as the glass substrate. This is proof of the smaller amount of polar distribution of all the optical sensor layers and the hydrophobic character of all the optical sensor layers. All the polar contribution in the case of the optical sensor layers is because of the presence of C-OH groups, which are present in a small amount. Electron donor contributions are smaller by around 80% in the case of optical sensor layers prepared with coating techniques and by more than 90% in the case of optical sensor layers prepared with inkjet printing. The O/C ratio of all the optical sensor layers is smaller by 52.1% in the case of optical sensor layers prepared with coating techniques and by 47% in the case of optical sensor layers prepared with inkjet printing. Meanwhile, the total SFE of optical sensor layers also decreased by around 45% and 37% in the case of optical sensor layers prepared with coating techniques and inkjet printing, respectively.

If we compare all the optical sensor layers, we can conclude that optical sensor layers prepared with coating techniques have almost identical surfaces with the same total SFE, the same Lifchitz–van der Waals contribution and the same electron donor and electron acceptor contribution. Optical sensor layers prepared with inkjet printing have higher total SFE, higher Lifchitz–van der Waals contribution and smaller electron donor and electron acceptor contribution compared to optical sensor layers prepared with coating techniques. Optical sensor layers prepared with inkjet printing also have the highest O/C ratio and the highest amount of C-C bonds and the smallest amount of C-OH and C-Si groups.

### 3.2.4. Spectral Properties of Sensor Layers in the Presence of Ammonia Response to Ammonia in an Aqueous Medium

The response to ammonia was determined through absorbance measurements of optical sensor layers in different concentrations of ammonia. The results are represented in Figures 5 and 6.

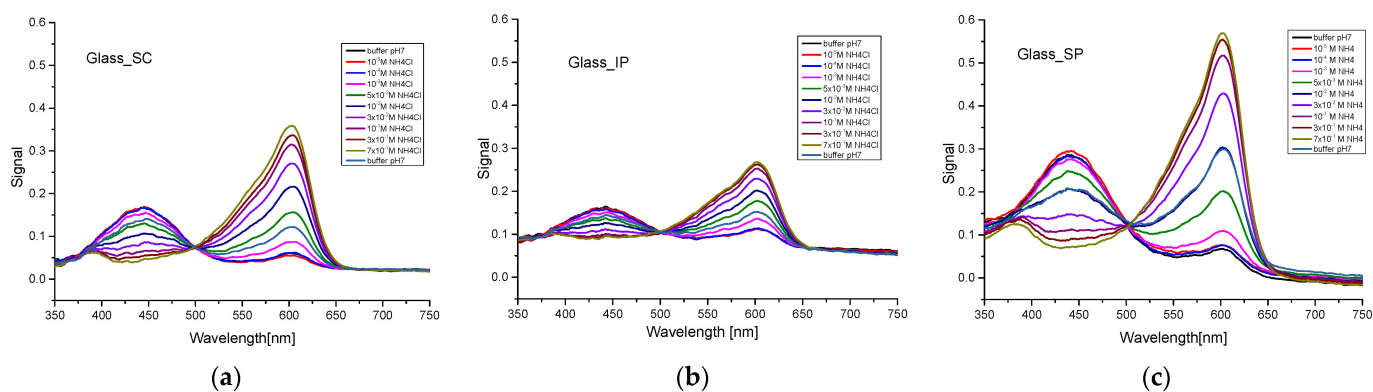


**Figure 5.** Spectral properties of sensor layers (SC, IP, SP) in the presence of dissolved  $\text{NH}_3$ . (a) Glass\_SC, (b) Glass\_IP, (c) Glass\_SP.

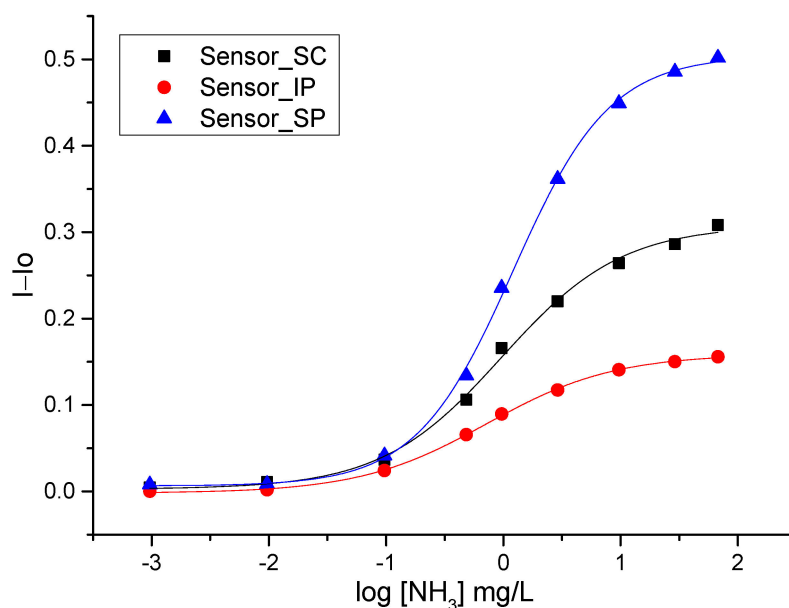


**Figure 6.** Calibration curves for optical sensor layers (SC, IP, SP) in the presence of dissolved  $\text{NH}_3$  in the concentration range  $1.0 \times 10^{-5}$  M– $7.0 \times 10^{-1}$  M.

Figure 5 presents the absorption spectra of the sensor layers prepared by the three different techniques; Figure 5a spin coating (SC), Figure 5b inkjet printing (IP), and Figure 5c spray coating (SP) in the presence of dissolved  $\text{NH}_3$  in the concentration range between  $1.0 \times 10^{-5}$  M and  $7.0 \times 10^{-1}$  M.

The sensor layers (SC, IP, SP) showed similar spectral properties in the presence of dissolved  $\text{NH}_3$  ( $1.0 \times 10^{-5}$  M– $7.0 \times 10^{-1}$  M). The intensity of the absorption peak at 600 nm (blue colour) increased in the presence of higher  $\text{NH}_3$  concentration, whereas the absorption peak between 400 and 460 nm (yellow colour) decreased. In the case of the sensor layer SP, the increase in the absorption peak at 600 nm is the highest, while in the case of IP, the increase is the smallest. Inkjet printing takes place at an elevated temperature and the sol-gel is probably more cross-linked and the dye less accessible, as a result, which is reflected in the response of the sensor coating, which in this case is the lowest. The difference between

spray and spin coating is due to the physically more accessible indicator in the case of spray coating. In spin coating, a lot of the sol-gel solution is dispersed during the spin itself, which results in less dye on the surface of the glass substrates. Unlike with spin coating, when spray coating is used, the solution is concentrated on a single point of the surface, which results in better accessibility of the dye, as is clearly visible in Figures 5c and 6.

For a better comparison of the most optimal sensor application for NH<sub>3</sub> detection, the spectral properties of the sensor layers (SC, IP, SP) are shown in Figure 6 as a function of different NH<sub>3</sub> concentrations at constant wavelength, which also shows the working range of NH<sub>3</sub> detection. The working range for the detection of dissolved NH<sub>3</sub> with the individual types of sensor layers (SC, IP, SP) is shown as a change in the absorbance signal at maximum absorbance ( $A_{\max} = 600 \text{ nm}$ ) as a function of the logarithmic values of the NH<sub>3</sub> concentrations. We can determine in which concentration range the sensor layers (SC, IP, SP) are most sensitive to the NH<sub>3</sub> or in which concentration range the signal change is directly proportional to the concentration of the dissolved NH<sub>3</sub>.

A comparison of the calibration curves showing absorbance as a function of logarithmic NH<sub>3</sub> concentration was performed between sensor layers produced by the three different techniques. As can be seen in Figure 6, the highest signal change of 0.5 in the presence of NH<sub>3</sub> is obtained with the sensor layer SP, while the lowest signal change of 0.16 occurred with the sensor layer IP. The sensor layer SC has a signal change of 0.3. For the sensor layer SP produced by spray coating, the signal change was 213% higher than the sensor layer IP produced by inkjet printing and 67% higher than the sensor layer SC produced by spin coating.

At lower concentrations of dissolved NH<sub>3</sub>, the optical SC and SP sensor layers have the same responsiveness. With increasing dissolved ammonia concentrations, responsiveness is higher for the optical sensor prepared with SP than for the optical sensor prepared with SC. The highest response to dissolved NH<sub>3</sub> is by the optical sensor layers prepared by spray coating ( $10^{-5} \text{ M}$ – $3 \times 10^{-1} \text{ M}$ ). Optical sensor layers prepared with inkjet printing (IP) are much less sensitive, especially in the lower concentration range of dissolved NH<sub>3</sub>.

If we compare the results in terms of manufacturing techniques, we can see that, in all three cases, optical sensor layers prepared with the three different techniques are responsive in the presence of low concentrations of dissolved NH<sub>3</sub> but deviations between them occur at higher concentrations. At higher concentrations, sensor layers prepared with spray coating (SP) techniques are more responsive and sensitive than the sensor layers prepared with the other two techniques (SC, IP).

#### Response Time of Sensor Layers (Time Drive)

The response time,  $t_{95}$ , of sensor layers prepared with different techniques was tested by continuous monitoring of absorbance changes at  $A_{\max} 600 \text{ nm}$  after the addition of NH<sub>4</sub>Cl ( $5 \times 10^{-3} \text{ M}$ ) in buffer pH7 solution. The results are represented in Figure 7.

Figure 7 shows the response time of three different sensor layers in the absence and presence of NH<sub>4</sub>Cl ( $5 \times 10^{-3} \text{ M}$ ). After exposure to the buffer solution signal was constant, when the sensor layer was exposed to the NH<sub>4</sub>Cl solution, the signal increased very steeply to an absorbance of 0.035 in the case of SP sensor layers and an absorbance of 0.01 in the case of the sensor layers SC and IP. After 30 min of exposure to the NH<sub>4</sub>Cl solution, the signal of the SP sensor layers had still not stabilized (with longer exposure the signal continued to increase). The SC and IP sensor layer signals stabilized after less than 10 min of exposure to the NH<sub>4</sub>Cl solution. When the buffer solution was reintroduced, the absorbance signal dropped almost to the original value in all three cases (SC, IP, SP). After the re-introduction of the NH<sub>4</sub>Cl solution (a further 30 min), the absorbance signal increased again to an even higher value than at the initial introduction of the solution. In the case of the SP layers, the absorbance value reached a value of 0.045, while in the case of SC and IP, the absorbance values were similar at 0.01. After the last cycle of introducing the buffer solution, the absorbance signal returned to almost the original value.

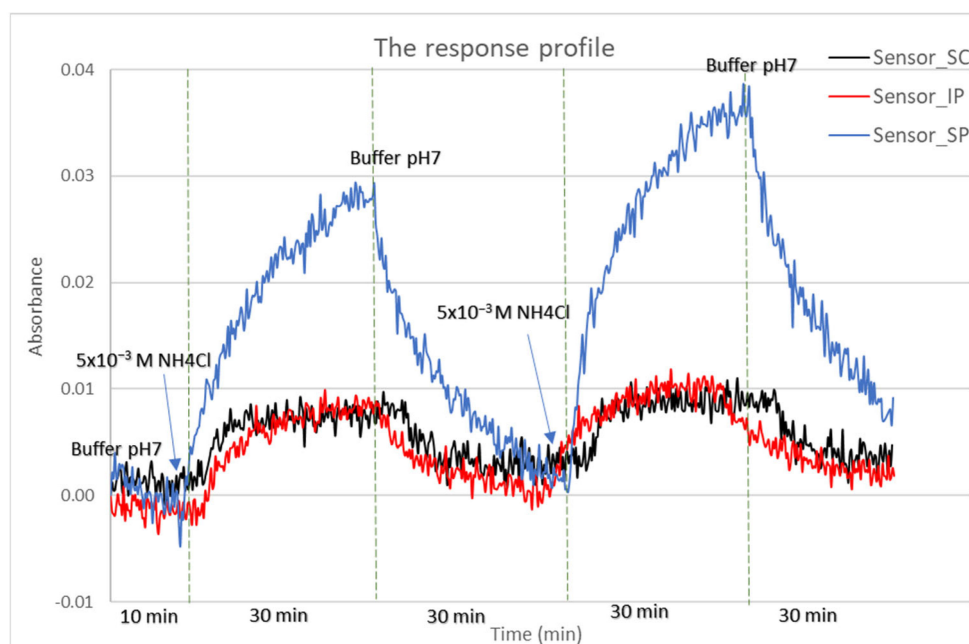


**Figure 7.** Response time of sensor layers (SC, IP, SP) in the presence of  $\text{NH}_4\text{Cl}$  ( $5 \times 10^{-3}$  M), pH 7.

The results obtained from response time measurement are comparable to the results from the response to dissolved  $\text{NH}_3$  in solution. With this measurement, we also proved that the optical sensor layers prepared with the SP technique have a higher response compared to sensors prepared with the other two techniques (SC, IP). The sensor layers SC and IP have a much lower response.

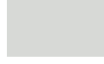
### 3.2.5. Real-Time Response of Optical Sensor Layers

The real-time response of the prepared optical sensor layers (SC, IP, SP) was evaluated using EOPTIS CLM19x colourimeter analysis based on the colour change. Optical sensor layers were exposed to fresh fish (from the market) in a closed container under real conditions in the refrigerator over time (6 days). The colour change in the sensor layers was monitored and measured daily. The colour change in the sensor layers is the result of a reaction between the indicator inside the sensor layers and the analyte, which is released during the ageing of the fish meat. When the fish is fresh, the colour of the sensor layers is yellow and when the fish is spoiled, the colour changes from yellow to blue. The results of the colourimetric analysis of the different optical sensor layers are summarized in Table 5 and graphically shown in Figure 8.

From Table 5, we can see that all three sensor coatings (SC, IP, SP) in the presence of analyte vapour show a colour change over time. The best response in terms of the largest colour change is shown by the SP sensor layers, which can also be seen in Figure 8. In these cases, the colour changed from yellow to green, and, finally, to blue, which indicates spoiled fish with a very bad smell. In the case of the SC optical sensor layers, the colour changes from yellow to green. On the last day, when the fish was spoiled, the sensor layers were still green. The IP sensor layers prepared with the inkjet printing technique were brighter compared to the other two techniques (SC, SP). In this case, the colour change went from yellow to light green.

To summarize, sensor layers prepared with the spray coating (SP) technique give the best results in terms of maximum colour change in the presence of analyte vapour released during spoilage of fish meat. When the fish was spoiled, the SP sensor layers were clearly blue, while the IP and SC sensor layers were still green.

**Table 5.** Colour changes (dEab\*) of sensor layers (SC, IP, SP) in the presence of fish meat over time.

	SC_Sensor		IP_Sensor		SP_Sensor	
	dEab*	Colour	dEab*	Colour	dEab*	Colour
Day 0	1.13		1.19		1.46	
Day 1	1.69		1.53		7.7	
Day 2	1.93		2.03		8.12	
Day 3	5.3		2.8		14.9	
Day 4	4.07		3.66		20	
Day 5	8.14		2.92		23.27	
Day 6	9.25		4.17		27.38	

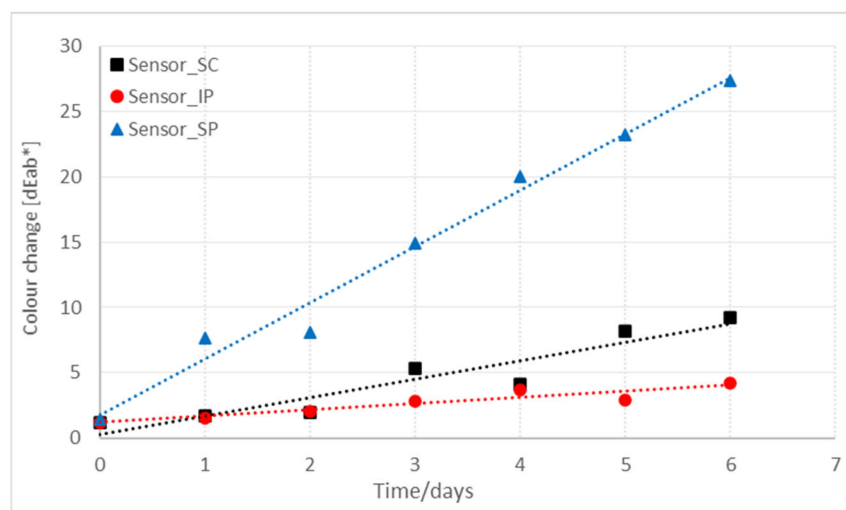
**Figure 8.** Colour change of three different sensor layers (SC, IP, SP) in the presence of fish meat over time.

Figure 8 is a graphical representation of the measurement results from Table 5. We can see that the smallest colour change was determined in the case of optical sensor layers prepared by inkjet printing (IP), a larger colour change was determined in the case of optical sensor layers prepared by spin coating (SC), and the biggest colour change was determined in the case of optical sensor layers prepared by spray coating (SP). These results are very comparable to those obtained in an aqueous medium represented by the calibration curves in Figure 6. In all cases, the sensor receptor prepared with the spraying technique (SP) shows a better response in the presence of the analyte.

#### 4. Conclusions

In this study, three different preparation methods (spin coating, inkjet printing and spray coating) of optical sensor layers were used to verify surface properties and responsiveness to ammonia. ATR-FTIR spectroscopy confirmed that the glass substrate was

successfully covered with a solution with the presentation of the same functional groups on all optical sensor layers. The water contact angle (WCA) and surface free energy are the same for all the optical sensor layers, especially for optical sensor layers made with spin and spray coating. The WCA for the SC and SP optical sensor layers is around  $80^\circ$ , and for IP optical sensor layers is  $83^\circ$ . The surface free energy is also the same for the SC and SP optical sensor layers at  $29 \text{ mJ/m}^2$ , while for the IP optical sensor layer, it is  $34 \text{ mJ/m}^2$ . All the optical sensor layers have the same surface elemental composition (with an atomic proportion of C of around 63 at. %, O of 23 at. %, and Si of 14 at. %) and the same amounts of differently bound carbons (C1 = 91%; C2 = 9%, and without C4).

Although all the surface properties are the same, all the optical sensor layers (SC, IP, SP) have different responses to dissolved  $\text{NH}_3$  solution and different responses in real-time measurements (exposure to fresh fish). If we compare results from the response of the optical sensor layers (SC, IP, SP) in the presence of dissolved  $\text{NH}_3$  in an aqueous solution according to the manufacturing technique, we can see that all the optical sensor layers are responsive at low concentrations. At higher concentrations, the SP sensor layers are more responsive and sensitive than the SC and IP sensor layers, which are, at higher concentrations, much less sensitive.

A similar response of the three different sensor layers (SC, SP, IP) was also confirmed by time-drive measurements in the presence of  $\text{NH}_4\text{Cl}$  solution in buffer media and by colourimetric analysis of sensor layers in the presence of a real sample, fish meat. The higher response over time and the biggest colour change were found with the SP sensor layers. Only the SP optical sensor layers changed colour from yellow, through green, to blue when the fish was spoiled. In the case of the other two layers (SC, IP), blue was not reached. We can conclude that the spray coating technique is the best for the optical sensor layers preparation for amine compound determination applications.

**Author Contributions:** Conceptualization, N.D., P.N. and A.F.P.A.M.R.; Methodology, N.D. and A.L.; Formal analysis, N.D. and P.N.; Investigation, N.D. and A.F.P.A.M.R.; Supervision, A.L.; Project administration, A.L. All authors have read and agreed to the published version of the manuscript.

**Funding:** This research was funded by the Ministry of Education, Science and Sport, Republic of Slovenia and European Union, European Regional Development Fund (ERDF), Early Research Careers 2.1 (Contract No. C3330-19-952032). The research work was also conducted within the framework of the Research Program P2-0438 Optical chemical/biosensor systems (OPTISENS). This work is also supported by an international research project, the Marie Skłodowska-Curie Action Global Mercury Observation and Training Network in Support to the Minamata Convention, financed under the funding line “excellent science” of the Horizon 2020 research and innovation program of the European Commission under the Marie Skłodowska-Curie grant agreement no. 860497.

**Institutional Review Board Statement:** Not applicable.

**Informed Consent Statement:** Not applicable.

**Data Availability Statement:** Data available on request due to commercial restrictions.

**Acknowledgments:** We also want to thank Miran Mozetič and Janez Kovač from the Institute Jožef Stefan for the XPS measurements and their interpretation.

**Conflicts of Interest:** The authors declare no conflict of interest.

## References

1. Enríquez, E.; de La Rubia, M.Á.; González, F.; Albuquerque, A.; Fernández, J.F. Effective Air-Spray Deposition of Thin Films Obtained by Sol-Gel Process onto Complex Pieces of Sanitary Ware. *J. Am. Ceram. Soc.* **2016**, *99*, 72–78. [[CrossRef](#)]
2. Kaloumenou, M.; Skotadis, E.; Lagopati, N.; Efstathopoulos, E.; Tsoukalas, D. Breath Analysis: A Promising Tool for Disease Diagnosis—The Role of Sensors. *Sensors* **2022**, *22*, 1238. [[CrossRef](#)]
3. Jerónimo, P.C.A.; Araújo, A.N.; Conceição, M. Optical sensors and biosensors based on sol-gel films. *Talanta* **2007**, *72*, 13–27. [[CrossRef](#)] [[PubMed](#)]
4. Barczak, M.; McDonagh, C.; Wencel, D. Micro- and nanostructured sol-gel-based materials for optical chemical sensing (2005–2015). *Microchim. Acta* **2016**, *183*, 2085–2109. [[CrossRef](#)]

5. Zhang, J.; Zhou, L. Preparation and Optimization of Optical pH Sensor Based on Sol-Gel. *Sensors* **2018**, *18*, 3195. [[CrossRef](#)]
6. Biring, S.; Sadhu, A.S.; Deb, M. An Effective Optical Dual Gas Sensor for Simultaneous Detection of Oxygen and Ammonia. *Sensors* **2019**, *19*, 5124. [[CrossRef](#)] [[PubMed](#)]
7. Matsuura, S.; Yamasaku, N.; Nishijima, Y.; Okazaki, S.; Arakawa, T. Characteristics of Highly Sensitive Hydrogen Sensor Based on Pt-WO<sub>3</sub>/Si Microring Resonator. *Sensors* **2020**, *20*, 96. [[CrossRef](#)]
8. Duong, H.D.; Rhee, J. Development of Ratiometric Fluorescence Sensors Based on CdSe/ZnS Quantum Dots for the Detection of Hydrogen Peroxide. *Sensors* **2019**, *19*, 4977. [[CrossRef](#)]
9. Steirer, K.X.; Berry, J.J.; Reese, M.O.; van Hest, M.F.; Miedaner, A.; Liberatore, M.W.; Collins, R.; Ginley, D.S. Ultrasonically sprayed and inkjet printed thin film electrodes for organic solar cells. *Thin Solid Films* **2009**, *517*, 2781–2786. [[CrossRef](#)]
10. Aziz, F.; Ismail, A.F. Spray coating methods for polymer solar cells fabrication: A review. *Mater. Sci. Semicond. Process.* **2015**, *39*, 416–425. [[CrossRef](#)]
11. Park, S.Y.; Kang, Y.-J.; Lee, S.; Kim, D.-G.; Kim, J.-K.; Kim, J.H.; Kang, J.-W. Spray-coated organic solar cells with large-area of 12.25 cm<sup>2</sup>. *Sol. Energy Mater. Sol. Cells* **2011**, *95*, 852–855. [[CrossRef](#)]
12. Peřinka, N.; Drřková, M.; Randjelović, D.V.; Bondavalli, P.; Hajná, M.; Bober, P.; Syrový, T.; Bonnassieaux, Y.; Stejskal, J. Characterization of Polyaniline-Based Ammonia Gas Sensors Prepared by Means of Spray Coating and Ink-Jet Printing. *Sens. Lett.* **2014**, *12*, 1620–1627. [[CrossRef](#)]
13. Kangur, T.; Nurmis, L.; Järvekülg, M. Influence of some system parameters on silica surface patterns by sol-gel phase separation method. *IOP Conf. Ser. Mater. Sci. Eng.* **2013**, *49*, 012035. [[CrossRef](#)]
14. Peřinka, N.; Drřková, M.; Randjelović, D.V.; Bondavalli, P.; Hajná, M.; Bober, P.; Syrový, T.; Bonnassieaux, Y.; Stejskal, J. Application of Ink-Jet Printing and Spray Coating for the Fabrication of Polyaniline/Poly(N-Vinylpyrrolidone)-Based Ammonia Gas Sensor. *Key Eng. Mater.* **2015**, *644*, 61–64. [[CrossRef](#)]
15. Gonzalez-Macia, L.; Morrin, A.; Smyth, M.R.; Killard, A.J. Advanced printing and deposition methodologies for the fabrication of biosensors and biodevices. *Analyst* **2010**, *135*, 845–867. [[CrossRef](#)]
16. Komuro, N.; Takaki, S.; Suzuki, K.; Citterio, D. Inkjet printed (bio)chemical sensing devices. *Anal. Bioanal. Chem.* **2013**, *405*, 5785–5805. [[CrossRef](#)]
17. De Gans, B.-J.; Duineveld, P.C.; Schubert, U.S. Inkjet Printing of Polymers: State of the Art and Future Developments. *Adv. Mater.* **2004**, *16*, 203–213. [[CrossRef](#)]
18. Monton, M.R.N.; Forsberg, E.M.; Brennan, J.D. Tailoring sol-gel-derived silica materials for optical biosensing. *Chem. Mater.* **2012**, *24*, 796–811. [[CrossRef](#)]
19. Zakir Hossain, S.M.; Luckham, R.E.; Smith, A.M.; Lebert, J.M.; Davies, L.M.; Pelton, R.H.; Filipe, C.D.M.; Brennan, J.D. Development of a bioactive paper sensor for detection of neurotoxins using piezoelectric inkjet printing of sol-gel-derived bioinks. *Anal. Chem.* **2009**, *81*, 5474–5483. [[CrossRef](#)]
20. Mensing, J.P.; Wisitsoraat, A.; Tuantranont, A.; Kerdcharoen, T. Inkjet-printed sol-gel films containing metal phthalocyanines/porphyrins for opto-electronic nose applications. *Sens. Actuators B Chem.* **2013**, *176*, 428–436. [[CrossRef](#)]
21. Di Risio, S.; Yan, N. Piezoelectric ink-jet printing of horseradish peroxidase: Effect of ink viscosity modifiers on activity. *Macromol. Rapid Commun.* **2007**, *28*, 1934–1940. [[CrossRef](#)]
22. Omar, S.; Pellice, S.; Ballarre, J.; Céré, S. Hybrid Organic-inorganic Silica-based Coatings Deposited by Spray Technique. *Procedia Mater. Sci.* **2015**, *9*, 469–476. [[CrossRef](#)]
23. Garcia, R.B.R.; Silva, F.S.; Kawachi, E.Y. Evaluation of dip and spray coating techniques in corrosion inhibition of AA2024 alloy using a silicon/zirconium sol-gel film as coating. *AIP Conf. Proc.* **2017**, *1809*, 020017. [[CrossRef](#)]
24. Carey, T.; Jones, C.; le Moal, F.; Deganello, D.; Torrisi, F. Spray-Coating Thin Films on Three-Dimensional Surfaces for a Semitransparent Capacitive-Touch Device. *ACS Appl. Mater. Interfaces* **2018**, *10*, 1994–19956. [[CrossRef](#)]
25. Arun Kumar, K.D.; Valanarasu, S.; Ponraj, J.S.; Fernandes, B.J.; Shkir, M.; AlFaify, S.; Murahari, P.; Ramesh, K. Effect of Er doping on the ammonia sensing properties of ZnO thin films prepared by a nebulizer spray technique. *J. Phys. Chem. Solids* **2020**, *144*, 109513. [[CrossRef](#)]
26. Chen, X.; Dai, Y.; Li, Z.; Zhang, Z.; Wang, X. Optical rubbery ormosils sensor for the detection of ammonia. *Fresenius J. Anal. Chem.* **2001**, *370*, 1048–1051. [[CrossRef](#)]
27. Fahad, O.A.; Mohammed, A.S. Thin films of tungsten oxide based on NH<sub>3</sub> and NO<sub>2</sub> gas sensors. *Mater. Today Proc.* **2021**, *42*, 2405–2409. [[CrossRef](#)]
28. Kundu, S.; George, S.J.; Kulkarni, G.U. Parts per billion sensitive, highly selective ambient operable, ammonia sensor with supramolecular nanofibres as active element. *Sens. Actuators B Chem.* **2021**, *347*, 130634. [[CrossRef](#)]
29. Deshpande, N.G.; Gudage, Y.G.; Sharma, R.; Vyas, J.C.; Kim, J.B.; Lee, Y.P. Studies on tin oxide-intercalated polyaniline nanocomposite for ammonia gas sensing applications. *Sens. Actuators B Chem.* **2009**, *138*, 76–84. [[CrossRef](#)]
30. Markovics, Á.; Kovács, B. Fabrication of optical chemical ammonia sensors using anodized alumina supports and sol-gel method. *Talanta* **2013**, *109*, 101–106. [[CrossRef](#)]
31. Tang, H.; Yan, M.; Zhang, H.; Li, S.; Ma, X.; Wang, M.; Yang, D. A selective NH<sub>3</sub> gas sensor based on Fe<sub>2</sub>O<sub>3</sub>-ZnO nanocomposites at room temperature. *Sens. Actuators B Chem.* **2006**, *114*, 910–915. [[CrossRef](#)]
32. Mani, G.K.; Rayappan, J.B.B. A highly selective room temperature ammonia sensor using spray deposited zinc oxide thin film. *Sens. Actuators B Chem.* **2013**, *183*, 459–466. [[CrossRef](#)]

33. Van Oss, C.J.; Chaudhury, M.K.; Good, R.J. Interfacial Lifshitz-van der Waals and Polar Interactions in Macroscopic Systems. Available online: <https://pubs.acs.org/sharingguidelines> (accessed on 30 January 2022).
34. Mohan, T.; Kargl, R.; Doliška, A.; Vesel, A.; Köstler, S.; Ribitsch, V.; Stana-Kleinschek, K. Wettability and surface composition of partly and fully regenerated cellulose thin films from trimethylsilyl cellulose. *J. Colloid Interface Sci.* **2011**, *358*, 604–610. [[CrossRef](#)] [[PubMed](#)]
35. Moulder, J.F.; Stickle, W.F.; Sobol, P.E.; Bomben, K.D. *Handbook of X-ray Photoelectron Spectroscopy: A Reference Book of Standard Spectra for Identification and Interpretation of XPS Data*; Chastain, J., Jr., Ed.; Physical Electronics: Chanhassen, MN, USA, 1995; Available online: <https://search.library.wisc.edu/catalog/999931119402121> (accessed on 30 January 2022).
36. Serra, J.; González, P.; Liste, S.; Serra, C.; Chiussi, S.; León, B.; Pérez-Amor, M.; Ylänen, H.; Hupa, M. FTIR and XPS studies of bioactive silica based glasses. *J. Non Cryst. Solids* **2003**, *332*, 20–27. [[CrossRef](#)]
37. Capeletti, L.B.; Zimnoch, J.H. Fourier Transform Infrared and Raman Characterization of Silica-Based Materials. In *Applications of Molecular Spectroscopy to Current Research in the Chemical and Biological Sciences*; InTech: London, UK, 2016. [[CrossRef](#)]
38. Li, Y.-S.; Wang, Y.; Ceesay, S. Vibrational spectra of phenyltriethoxysilane, phenyltrimethoxysilane and their sol–gels. *Spectrochim. Acta A Mol. Biomol. Spectrosc.* **2009**, *1819*, 71–1824. [[CrossRef](#)] [[PubMed](#)]
39. Deng, X.M.; Castillo, E.J.; Anderson, J.M. Surface modification of soft contact lenses: Silanization, wettability and lysozyme adsorption studies. *Biomaterials* **1986**, *7*, 247–251. [[CrossRef](#)]
40. Stuart, B.H. *Infrared Spectroscopy: Fundamentals and Applications*; John Wiley: Chichester, UK; Hoboken, NJ, USA, 2004; Available online: <https://search.library.wisc.edu/catalog/999974109102121> (accessed on 30 January 2022).
41. Nordin, N.; Ahmad, Z. Monitoring chemical changes on the surface of borosilicate glass covers during the silanisation process. *J. Phys. Sci.* **2015**, *26*, 11–22.
42. Kangur, T.; Kiisk, V.; Loot, A.; Timusk, M.; Järvekülg, M. Optical functionality of micro- and nanostructured silica surfaces prepared by a sol-gel phase separation method. *Thin Solid Films* **2017**, *622*, 11–16. [[CrossRef](#)]

**Disclaimer/Publisher's Note:** The statements, opinions and data contained in all publications are solely those of the individual author(s) and contributor(s) and not of MDPI and/or the editor(s). MDPI and/or the editor(s) disclaim responsibility for any injury to people or property resulting from any ideas, methods, instructions or products referred to in the content.